HEALTH AND MEDICINE

Surface-anchored framework for generating RhD-epitope stealth red blood cells

Yueqi Zhao[1]*, Mingjie Fan[2,3]*, Yanni Chen[2,3], Zhaoming Liu[1], Changyu Shao[1], Biao Jin[1], Xiaoyu Wang[4], Lanlan Hui[2,3], Shuaifei Wang[5,6], Zhaoping Liao[7], Daishun Ling[5], Ruikang Tang[1,4†], Ben Wang[2,3†]

Rhesus D (RhD) is one of the most important immunogenic antigens on red blood cells (RBCs). However, the supply of RhD-negative blood frequently faces critical shortages in clinical practice, and the positive-to-negative transition of the RhD antigen remains a great challenge. Here, we developed an alternative approach for sheltering the epitopes on RhD-positive RBCs using a surface-anchored framework, which is flexible but can achieve an optimal shield effect with minimal physicochemical influence on the cell. The chemical framework completely obstructed the RhD antigens on the cell surface, and the assessments of both blood transfusion in a mouse model and immunostimulation with human RhD-positive RBCs in a rabbit model confirmed the RhD-epitope stealth characteristics of the engineered RBCs. This work provides an efficient methodology for improving the cell surface for universal blood transfusion and generally indicates the potential of rationally designed cell surface engineering for transfusion and transplantation medicine.

INTRODUCTION

The pioneering studies of Karl Landsteiner in the 19th century laid the foundation of our current understanding of blood types (*1*). The major human alloantigen system involves the ABO, Rhesus (Rh), MNS, Lutheran, and Kell blood groups, among others (*2*). The Rh blood group system is a clinically notable human blood group polymorphism in alloimmunization (*3*) and includes more than 50 different serologic specificities (*4*), which makes this system particularly important and challenging for biomedical scientists and clinicians. Within the Rh blood group, the D antigen is the most immunogenic and clinically important epitope (*5*). Approximately 85%, 95%, and greater than 99.5% of Caucasians, black Africans, and East Asians have RhD-positive blood, respectively (*2*). As a rare blood type, there is a critical shortage and extremely inadequate supply of RhD-negative blood for transfusion, especially in emergencies (*6*). Exposure of RhD-negative individuals to RhD-positive blood may cause serious immune responses, including hemolysis, which is life threatening (*3*).

Converting RhD-positive blood to RhD-negative blood may be a feasible strategy for the development of a potential therapeutic modality but represents a significant challenge. Enzymatic removal of red blood cell (RBC) antigens can be successfully applied to convert type A or B RBCs into type O RBCs (*7*, *8*). However, this process is not related to the immunogenic epitopes of the Rh antigens, which are intrinsically associated with RBC membranes. Deletion of the Rh-related polypeptides would result in the disintegration of the entire cell membrane (*9*). Using a proof-of-concept method, nuclease-based editing of blood group–determining genes can lead to the conversion of D-positive cells into D-negative cells (*10*). However, this editing may cause unexpected mutation and in vivo evaluations have not been carried out. Another potential strategy for RBC modification is cell encapsulation using chemical polymer camouflages (*11*–*15*). However, polymer-based "molecular brush" camouflage is always incomplete, and this technology has not been further developed. Although some biomimetic molecules, such as polydopamine (PDA) (*16*), can achieve site-to-site shielding against the antigens on RBCs, this treatment always leads to a notable decrease in membrane fluidity so that the modified cells are readily disrupted due to increased cell fragility. Specifically, balancing efficient epitope shielding and cell fragility using PDA is critical. Here, we developed a new technique to engineer cell surfaces for the production of RhD-negative RBCs using a rationally designed three-dimensional (3D) crosslinking framework of polysialic acid (PSA)–tyramine hydrogel, which has a flexible texture to ensure cell membrane stability. The new technique for the anchored framework can balance the modified RBC membrane fluidity and RhD antigen shielding and achieves successful transfusion of the engineered RhD-positive RBCs to RhD-negative recipients without immunogenicity for the first time (Fig. 1).

RESULTS

Construction of the 3D framework on individual RBCs

This technique involves a horseradish peroxidase (HRP)–catalyzed synthesis method that results in the encapsulation of individual cells within a nanogel framework (Fig. 2A). We used a conjugate of HRP and a biocompatible anchor molecule (BAM) on cell membranes (BAM-HRP) (fig. S1A) to immobilize HRP on the cell surface (Fig. 2B) (*17*). BAM is a single oleyl chain derivative coupled with hydrophilic poly(ethylene glycol) (PEG) (*18*). Individual cells were engineered with crosslinking frameworks constructed from PSA and tyramine through the reaction of H_2O_2 catalyzed by HRP enzymes (Fig. 2C), which was immobilized on the cell surface. Because PSA might play

[1]Center for Biomaterials and Biopathways, Department of Chemistry, Zhejiang University, Hangzhou 310027, China. [2]Cancer Institute (Key Laboratory of Cancer Prevention and Intervention, China National Ministry of Education), The Second Affiliated Hospital, Zhejiang University School of Medicine, Hangzhou 310009, China. [3]Institute of Translational Medicine, Zhejiang University, Hangzhou 310029, China. [4]Qiushi Academy for Advanced Studies, Zhejiang University, Hangzhou 310027, China. [5]Institute of Pharmaceutics and Hangzhou Institute of Innovative Medicine, College of Pharmaceutical Sciences, Zhejiang University, Hangzhou 310058, China. [6]Affiliated Sir Run Run Shaw Hospital, School of Medicine, Zhejiang University, Hangzhou, China. [7]Department of Transfusion, The Second Affiliated Hospital, Zhejiang University School of Medicine, Hangzhou 310009, China.
*These authors contributed equally to this work.
†Corresponding author. Email: rtang@zju.edu.cn (R.T.); bwang@zju.edu.cn (B.W.)

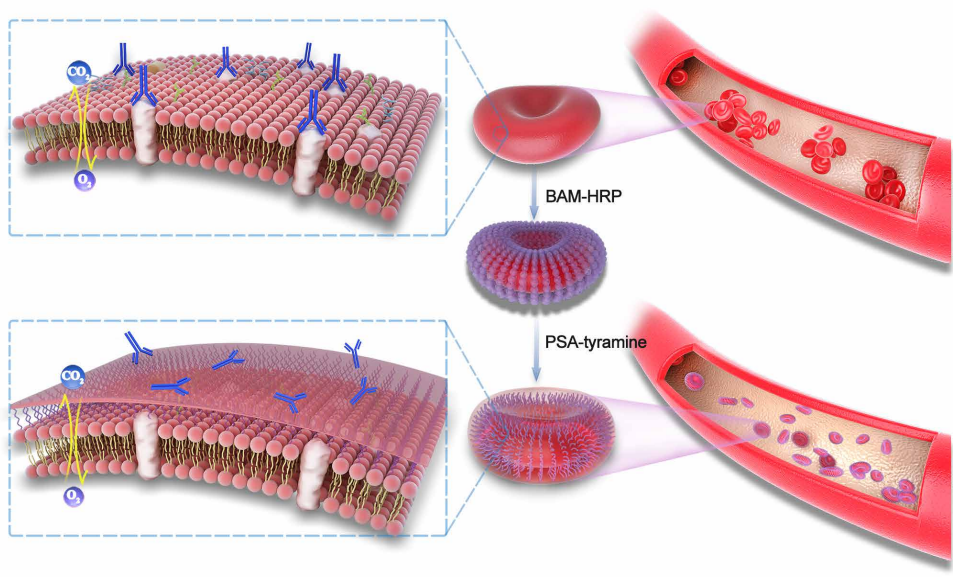

Fig. 1. Schematic illustration of the procedure for RBC surface engineering and the derived functions of individual cell-material hybrids in universal blood transfusions.

a significant role in the circulation time of erythrocytes, crosslinking with biogenic amines (tyramine) was used to form the 3D framework structure. Because the membrane-anchored 3D structure is flexible, we suggest that it may block the antigen-antibody recognition completely on the cell surfaces with reduced influence on cell fragility.

We engineered fully functionalized RBCs with sheaths of a PSA-tyramine nanogel layer for which the antigen determinants were camouflaged to prevent the recognition of the immune system. The synthesis of the crosslinking frameworks was performed using *N*-ethyl-*N*′-(3-dimethylaminopropyl)carbodiimide (EDC)/*N*-hydroxysuccinimide (NHS) conjugation chemistry (Fig. 2C), and the chemical structure of the synthesized PSA-tyramine conjugate was confirmed by ^{1}H nuclear magnetic resonance (NMR) (fig. S1B). With the formation of the PSA-tyramine conjugate, four double peaks arose between 7.32 and 6.73 parts per million (ppm) due to the benzene of tyramine and the complicated multiplets between 3.24 and 2.71 ppm belonging to the methylene groups of tyramine (*19*). The overall appearance of the native and engineered RBCs was smooth and relatively similar as analyzed by scanning electron microscopy (SEM) (Fig. 2, D and G). The surface engineering was successful, and an approximately 250-nm-thick apparent gel layer was observed on the engineered cell surface by transmission electron microscopy (TEM) (Fig. 2H) and confocal laser scanning microscopy (CLSM) (Fig. 2I). Conversely, the native RBCs were in a nongel layer and nonfluorescent (Fig. 2, E and F). Furthermore, amide formation in the surface modification process was detected by Fourier transform infrared (FTIR) spectroscopy, and the manifestation of the CO-NH peak indicated the formation of an N-H amide on the cell surface (fig. S1C) (*20*). The engineered RBCs with hydrogel anchored on the cell surface can be stored stably in human plasma over 8 days, and they present the same hemolysis profile of native RBCs (fig. S2).

Stealth effect of the 3D framework on blood recognition

To measure the serological reactivity on the engineered surface of RBCs, agglutination assays of native and engineered RBCs with anti-RhD sera were conducted. The agglutination of RhD-positive RBCs incubated with anti-RhD sera occurred accordingly and was identified by microscopy (Fig. 2J). In contrast, agglutination for engineered RBCs with anti-RhD sera disappeared, indicating that the surface-engineered framework on the RBCs successfully prevented the recognition of antigens with the respective antibodies (Fig. 2K). In addition, serological analysis of the other blood type sera (anti-A and anti-B) demonstrated that the chemical polymer camouflage was also effective for blood groups A and B (fig. S3, A to F). Moreover, flow cytometry using commercial anti-RhD monoclonal antibodies (4A Biotech) was used to evaluate the shielding condition of antigens by cell surface framework engineering. The native RhD-positive RBCs showed a positive rate of antibody affinity up to 100%, whereas that of the surface-engineered RBCs decreased to zero (Fig. 2L and fig. S3H). In addition, the Rh epitopes were exposed if the low concentration (0.25 mM) of PSA-tyramine was adopted during RBC surface engineering (fig. S3G). The circulation time in vivo was shorter (only 7 days) when a high concentration (1 mM) of hydrogel was used during the RBC surface engineering (fig. S3, I and J), and the clearance was believed to be influenced by changes in band 3 clustering (*9*). Thus, the rational framework composed of PSA-tyramine (0.5 mM) established an effective barrier against antigen-antibody reactions of the blood type and camouflaged the epitopes on the red cell surface. We performed additional experiments to compare BAM-HRP with other coating methods. Compared with this method, which achieves complete RhD antigen shielding while maintaining cell membrane fluidity, the other methods, such as BAM only, PSA brush, or PDA coating, cannot exhibit properly effective RhD shielding but may achieve type A and B antigen shielding (fig. S4).

Ideal function maintenance of framework-engineered RBCs

The physicochemical properties of both native and engineered RBCs were examined for comparison. Osmotic fragility was used to determine whether the cells were more fragile upon crosslinking cell surface engineering. Significant differences were not observed in the osmotic fragility curves of the engineered RBCs compared to the control cells, indicating that the modification process had good

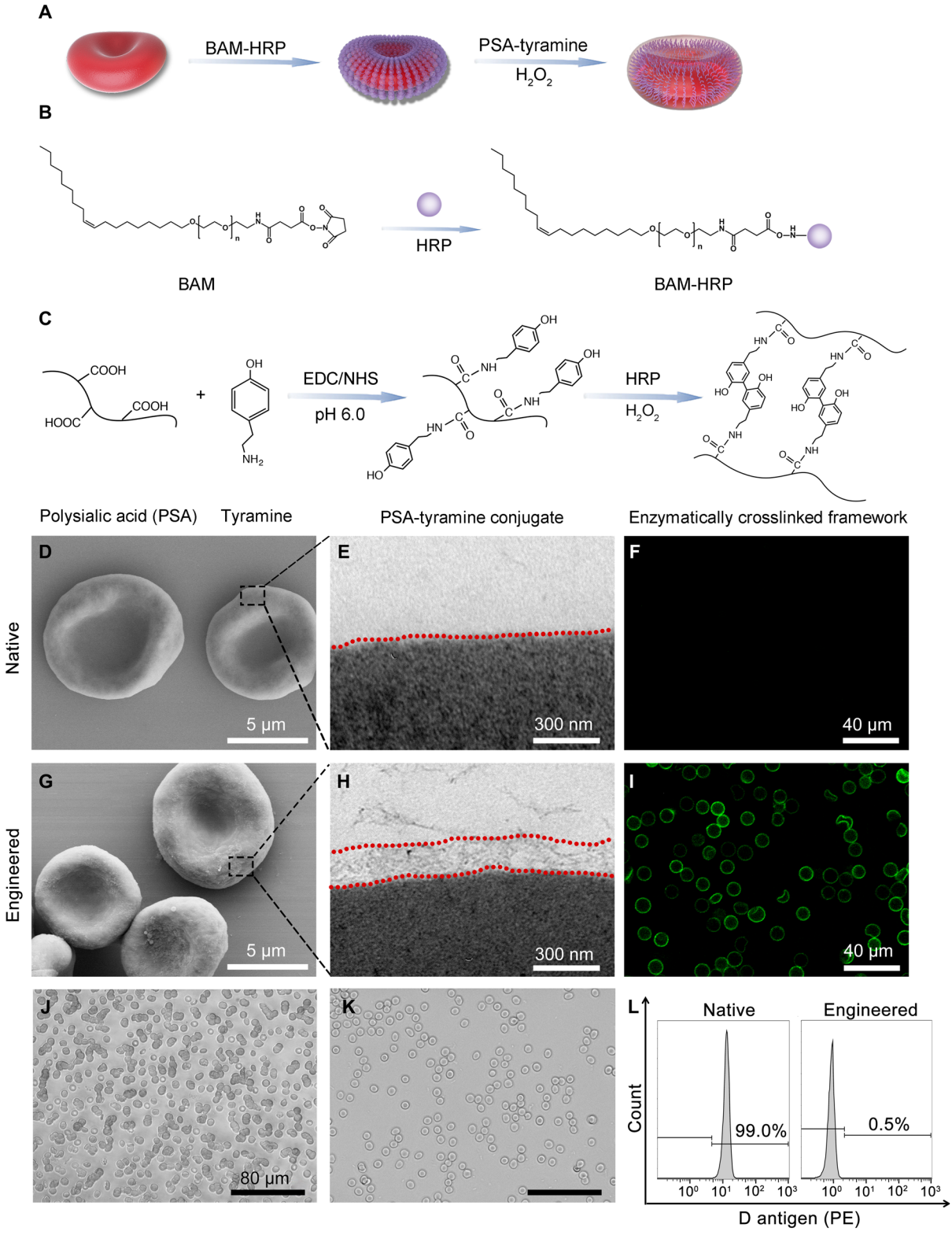

Fig. 2. Rational surface crosslinking framework for the construction of universal RBCs. (**A**) Schematic illustration of the procedure for RBC surface engineering. (**B**) Synthetic scheme for the anchor molecule conjugate (BAM-HRP). (**C**) Mechanism of the formation of PSA-tyramine conjugate and enzymatically crosslinked framework. SEM images of (**D**) human native RBCs and (**G**) surface-engineered human RBCs in the presence of BAM-HRP solution, PSA-tyramine (10 mg/liter), and H_2O_2 solution. TEM images of (**E**) human native RBCs and (**H**) surface-engineered human RBCs. Confocal images of (**F**) native RBCs and (**I**) engineered RBCs. (**J**) Optical images of human RhD-positive RBCs in the corresponding anti-typing sera. (**K**) BAM-tyramine-PSA engineered RhD-positive RBCs were mixed with equal concentrations of their anti-typing sera. (**L**) Flow cytometry analysis of native RBCs (left) and surface-engineered human RBCs (right) with fluorescein isothiocyanate–labeled anti-RhD antibodies.

compatibility for RBCs (Fig. 3A) (*21*). The contact angle measurements were performed by placing droplets of water on the native and sheltered RBC-coated substrates, and the values were 54.83 ± 5.87° and 48.42 ± 4.78°, respectively (Fig. 3B), indicating a nonsignificant difference in the hydrophobicity of the cell membrane after surface engineering. The zeta potential of the blood sample decreased slightly after modification (Fig. 3C), although significant differences were not identified by statistical analysis. Last, the availability of universal blood was illustrated with relatively constant physical properties but varying deformability by in vitro studies of the surface-engineered RBCs. The deformability of the native RBCs was greater than that of the crosslinking framework-shielded RBCs due to the nanoscale encapsulation (Fig. 3D). Because of the increased deformability, Young's modulus tests were used to compare the values of elasticity between the native blood samples and the modified cells. Cell surface engineering also enhanced Young's modulus of erythrocytes from 2.01 ± 0.89 kPa to 2.47 ± 1.87 kPa (fig. S5A).

To investigate whether cell surface engineering could retain the biological functions of RBCs in vitro, the engineered RBCs were characterized based on the P_{50}, Hill plot, 2,3-diphosphoglyceric acid (2,3-DPG), adenosine triphosphate (ATP), and adenosine triphosphatase (ATPase) parameters and then compared with native RBCs. Hb-oxygen affinity is a primary factor in determining tolerance to hypoxia. The oxygen dissociation curve (ODC) of Hb is of profound clinical importance and accounts for the oxygenation performance of Hb, which has physiological and clinical implications (*22*). The ODC between the native and engineered RBCs was similar (Fig. 3E), and the affinity of Hb for oxygen was more optimally measured by deriving the P_{50} value, which is the partial pressure of oxygen at which Hb is 50% saturated with oxygen. The P_{50} value slightly decreased from 25.81 ± 1.53 mmHg to 23.09 ± 0.25 mmHg (fig. S5B), which may be due to catalyzed oxidation resulting in the high oxygen affinity of Hb (*23*). Hb and methemoglobin (MetHb) have been investigated using a spectroscopic method, and ultraviolet-visible (UV-Vis) spectroscopy (Q band and Soret band) (*24*) showed that the engineered RBCs can also carry oxygen (fig. S5D). Meanwhile, the Bohr coefficient is defined here as the change in oxygen affinity with pH value, and it imitated the difference in proton binding between oxyhemoglobin and deoxyghemoglobin in the microenvironment and niche pH of lungs and muscle tissue. The Bohr coefficient

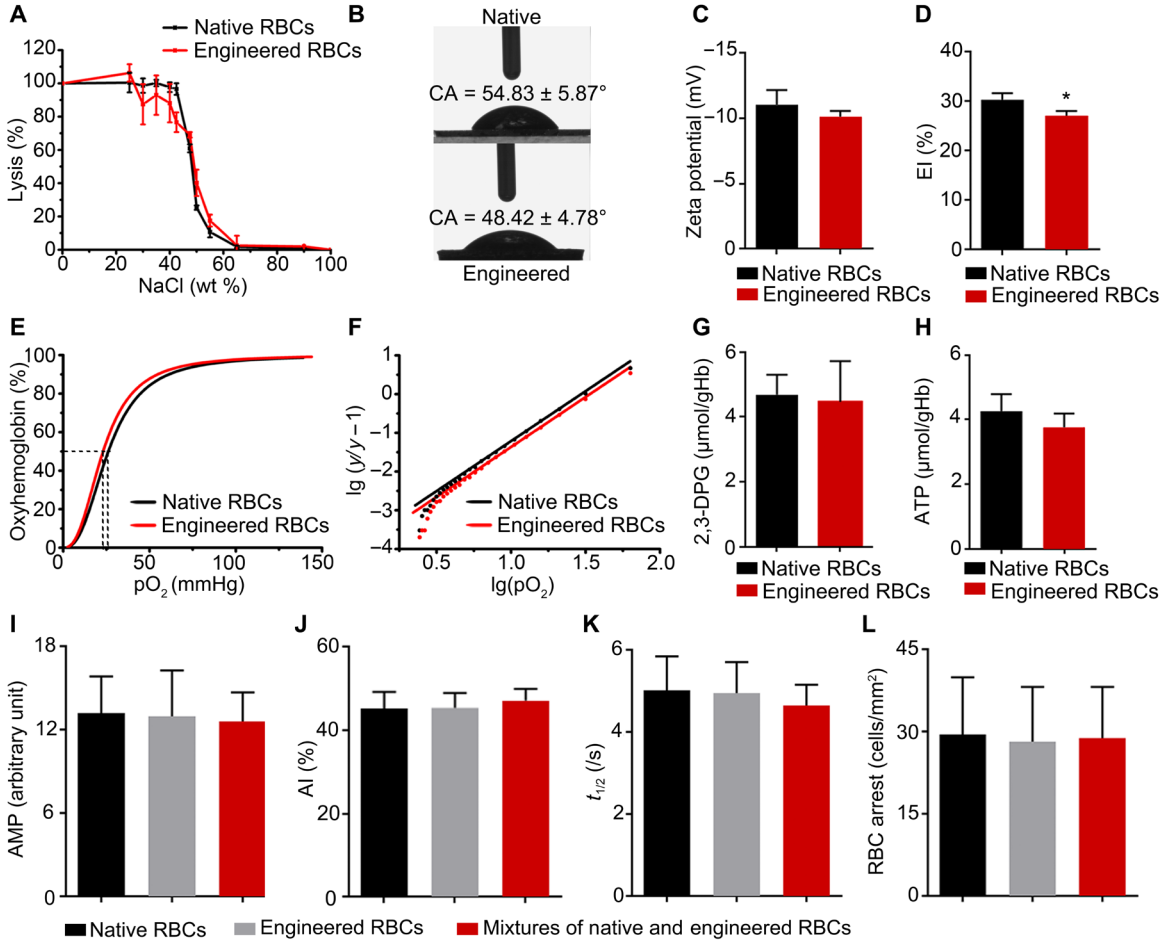

Fig. 3. Physiochemical properties and biofunctional analysis of the native and engineered RBCs. (**A**) Osmotic fragility at 1 hour after the grafting of native RBCs (black) and RBCs derivatized with tyramine-PSA (10 mg/ml) (red). (**B**) Hydrophobicity tests based on the contact angle of the cell monolayer. (**C**) Cell electrophoresis assay characterized by zeta potential. (**D**) Deformability of the RBCs tested by ektacytometry. (**E** to **H**) Structural and functional analysis of the native RBCs (black) and engineered RBCs (red), including the ODC and the contents of Hill plot, 2,3-DPG, and ATP. (**I** to **K**) AI, AMP, and $t_{1/2}$ of native RBCs, engineered RBCs, and mixtures of native and engineered RBCs in human plasma. (**L**) Comparison of the adhesions of the native RBCs, engineered RBCs, and mixtures of native and engineered RBCs to an endothelial cell–coated surface. a.u arbitary unit

maintained its full value when the antigens were sheltered, and the oxygen affinity was almost not affected (fig. S5, E and F) (*25*). Because the Hill coefficient did not vary with the modification of the cell membrane (Fig. 3F), we deduced that the surface-engineered RBCs would not impact their unique function of transporting oxygen. 2,3-DPG appears to be an important regulator of the ODC of Hb in intact RBCs (*26*). The 2,3-DPG content did not change before and after cell surface engineering, and the values were 4.68 ± 0.59 μmol/gHb and 4.52 ± 1.31 μmol/gHb, respectively (Fig. 3G). We also noticed an equivalent ATP output from 4.27 ± 0.48 μmol/gHb to 3.60 ± 0.69 μmol/gHb after the crosslinking treatment (Fig. 3H), which was essential in maintaining the biconcave shape of the RBC membrane (*27*). The ATPase content showed limited differences between the native and engineered RBCs, and the values were 43.35 ± 9.61 U/gHb and 45.00 ± 15.78 U/gHb, respectively (fig. S5C).

A consensus has not been reached on whether the homeostatic functions of aggregated RBCs are safe for transfusion due to the increased blood viscosity and reduced blood flow (*28*). The aggregate amplitude (AMP), aggregation index (AI), and aggregation half-time ($t_{1/2}$) of the native RBCs, engineered RBCs, and mixtures of native and engineered RBCs in human plasma were consistent (Fig. 3, I to K). The abnormal or enhanced adhesiveness of the RBCs to endothelial cells leads to various diseases (*29*). The engineered RBCs and mixtures of native and engineered RBCs show normal adhesion efficiency to endothelial cells similar to that of native RBCs (Fig. 3L). Normal blood clotting function is critical to the survival of transfusion recipients with actively bleeding injuries (*30*). Changes indicative of clot dynamics were not observed in these groups (fig. S5, G to J), as assessed using thrombelastography (TEG) parameters, the reaction time (R), the coagulation time (K), the α angle (α), and the maximum amplitude (MA).

All these results demonstrated that the surface engineering of RBCs adequately maintained the key functions of cells.

Framework-engineered RBCs in blood transfusion

To demonstrate that the crosslinking engineering on the RBC surfaces is functional in vivo, RBCs with or without surface modification were used to perform blood transfusion by caudal vein injections in mice for an extended time period. We visualized and quantified the circulation profiles of the native and engineered RBCs labeled by 1,1′-dioctadecyltetramethyl indotricarbocyanine iodide (DIR; GeneCopoeia) in different organs, including the heart, liver, spleen, and kidney, based on the imaging function of the photoacoustic system colocalized with oxyhemoglobin (red) and deoxyghemoglobin (blue) (fig. S6), and the results indicated that the labeled RBCs presented appropriate functions. Photoacoustic images of the RBC distribution in the whole body were captured at 4 hours, 5 days, 10 days, 15 days, and 20 days after injection, and the natural distribution was observed in different organs (Fig. 4, A to D). Both native and engineered RBCs showed increased intensity in the spleen and liver, which are known to be the main sites for blood storage compared with other organs, such as the heart and kidney. The long-term in vivo fate of the engineered RBCs in the blood circulation demonstrated that the engineered RBCs could remain present and in a normal state for more than 20 days (Fig. 4E). The oxyhemoglobin intensity of engineered RBCs labeled by DIR dye in the organs of treated mice had no significant difference compared with the control mice, confirming that surface engineering can competitively maintain blood oxygenation levels in vivo (Fig. 4F). Moreover, the life span of the engineered RBCs in blood circulation of 40 days was similar to that of the remaining native RBCs circulated in vivo (Fig. 4G). Histopathological studies of the main organs, such as the heart, liver, lung, spleen, and kidney, were further analyzed by hematoxylin and eosin (H&E) staining, and signatures of tissue damage were not observed (fig. S7). The routine blood test also confirmed that the interfacial framework engineering on RBCs could maintain the normality of treated mice after blood transfusion with engineered RBCs (table S1).

A multiple transfusion study (Fig. 5A) was performed in vivo to determine the transfusion capacity of engineered RBCs and examine the impact of transfused engineered RBCs on complement activation and cytokine response. The circulation periods of the three subsequent transfusions with the native and engineered RBCs were consistent (Fig. 5B). As depicted in Fig. 5A, the two groups had elevated levels of complement 3 and complement 4, verifying the lack of complement activation after the transfusion of the engineered RBCs (Fig. 5C). The serum levels of tumor necrosis factor–α (TNF-α) and interleukin-6 (IL-6) were normal, suggesting that surface engineering did not lead to an inflammatory effect (Fig. 5D). Blood tests were used for the initial assessment of liver injury, which included measuring the levels of serum alanine and aspartate aminotransferases (ALT and AST), alkaline phosphatase (ALP), and bilirubin (TBIL and DBIL). The serum enzyme levels and biochemical clues associated with bilirubin were in the normal range (Fig. 5E). Serum creatinine acid (CREA), blood urea nitrogen (BUN), and uric acid (UA) were used as indicators for kidney damage and have been used as a gold standard biomarker for evaluating acute renal injury. We found that the biochemical clues of renal function were not abnormal between the two groups (Fig. 5F).

We performed hemorrhagic tests in a mouse model and observed the recovery after blood transfusion. The heart rates (HRs) of the treated mice were heightened after removing 10% of the volume of native blood but rehabilitated after injecting native RBCs or engineered RBCs and remained at a normal condition over 1 hour of monitoring (fig. S8A). The mean blood pressure (MBP) and systolic blood pressure (SBP) were significantly decreased with hemorrhagic progression but gradually recovered after blood transfusion (fig. S8, B and C). Routine blood analyses were performed to investigate the systematic biosafety of blood transfusion with engineered RBCs, and abnormal parameters were not found (table S2).

These results indicated that surface engineering leads to negligible complement activation and cytokine response and presents good biocompatibility, thus confirming the translational potentials of this new approach in multiple transfusions.

Stealth RhD antigens of engineered RBCs in immunostimulation

Immunostimulation with RhD-positive human RBCs was conducted in a rabbit model, and the immunogenicity of the engineered RBCs was evaluated in vivo. According to the immunization schedule, rabbits with preexisting anti-RhD immunity were first primed on week 0 with human RhD-positive RBCs and then boosted at week 3 with human RhD-positive RBCs or engineered RBCs in groups 1 and 2, respectively. In contrast, the rabbits in groups 3 and 4 were primed with an injection of engineered RBCs and RhD-negative RBCs at weeks 0 and 3 separately as the positive control and negative control groups, respectively (Fig. 6A). Next, we examined whether the interfacial framework could influence the immune recognition

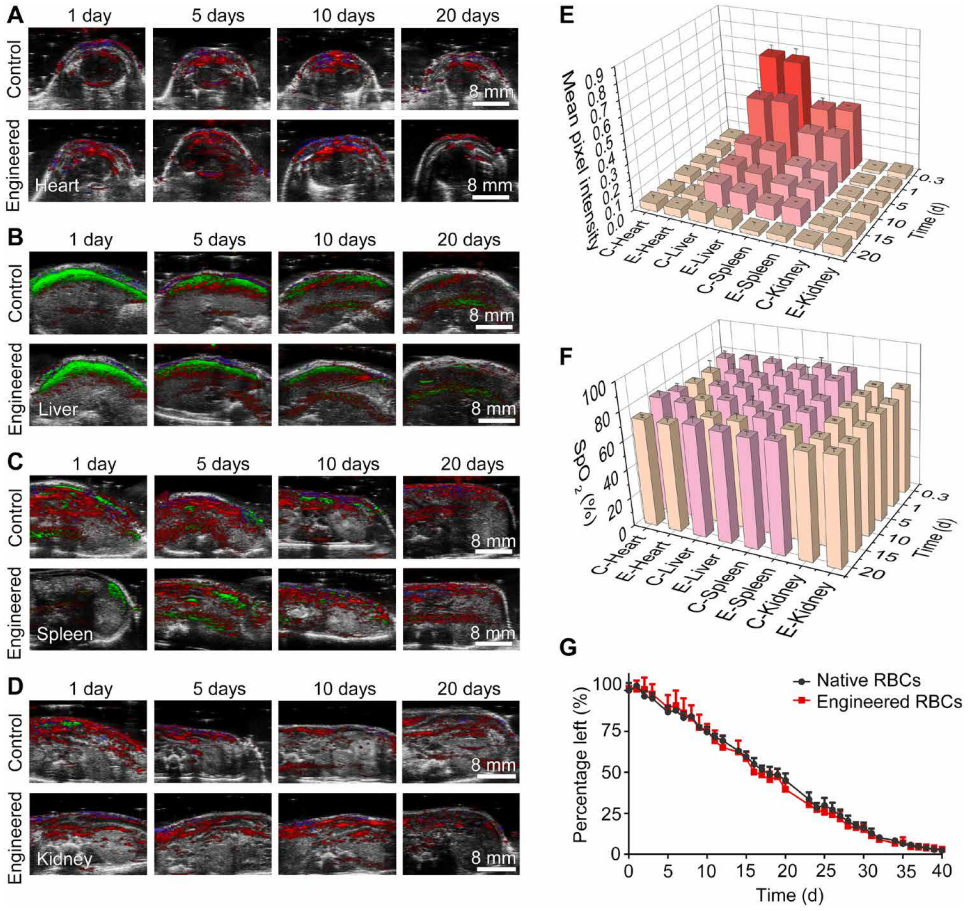

Fig. 4. Usable and functional in vivo assay of the distribution of engineered RBCs after blood transfusion in organs in a mouse model. (**A** to **D**) Photoacoustic images of a mouse's heart, liver, spleen, and kidney after injecting native and engineered RBCs labeled with DIR dye. Red, oxyhemoglobin; blue, deoxyhemoglobin; green, DIR dye. (**E**) Quantitative intensities of native and engineered RBCs labeled with DIR dye in the liver, spleen, and kidney after injection. (**F**) Quantitative intensity of oxyhemoglobin in the liver, spleen, and kidney after injection. (**G**) Survival profiles of PKH-26–labeled RBCs after blood transfusion in vivo.

of antibodies. The humoral immune responses of human RhD-positive RBCs and engineered RBCs were evaluated using an immunoglobulin G (IgG) enzyme-linked immunosorbent assay (ELISA). The results revealed that 3 weeks after immunization, the rabbits with preexisting anti-RhD immunity elicited comparable levels of RhD immune responses. However, no obvious RhD antigen-specific immune response was observed in the rabbits in group 3, which received two injections of the engineered RBCs, and no difference was observed relative to the negative control group (Fig. 6B, red and blue). To our surprise, the second injection of engineered RBCs presented a significant dampening effect on the RhD immune responses in group 2 in comparison with group 1, which received two injections of native human RhD-positive RBCs (Fig. 6B, black and gray). The peak in group 1 related to the RhD immune response was significantly boosted at week 5 compared with that of the other three groups (Fig. 6C). These results indicated that the crosslinking framework sheltered the epitopes of RBCs in vivo, suggesting the direct ablation of the molecular recognition between antigens and antibodies.

Furthermore, the systematic biosafety of engineered RBCs was investigated in rabbits, and the hepatotoxicity and kidney toxicity were assessed. The liver is the largest organ with interdependent metabolic, excretory, and defense functions. The serum enzyme levels of ALT, AST, and ALP and the biochemical indicators TBIL and DBIL were used to assess liver injury. Abnormalities in these biochemical profiles were not observed in the four groups after injections of native and engineered RBCs (Fig. 6D). The levels of CREA, BUN, and UA, which were used to evaluate acute renal injury, were in the normal range (Fig. 6E). These results indicated that surface modifications can not only bypass anti-RhD immunity but also promote favorable biocompatibility. Therefore, the engineered framework functioned as a structured adjuvant that allowed the complete avoidance of immune responses, thus ensuring a successful RhD-stealth blood transfusion.

DISCUSSION

Blood transfusion is the most common form of tissue transplantation, and blood type matching is required and generally the most critical point in transfusion medicine (*31*). Occasionally, appropriate donors for patients with rare blood types, such as RhD-negative RBCs, cannot be obtained on-site or quickly enough (*32*), which could result in life-threatening circumstances. Hb-based blood substitutes have been a hot research topic for some time; however, a safe and effective blood substitute has not been successfully developed to date (*33*).

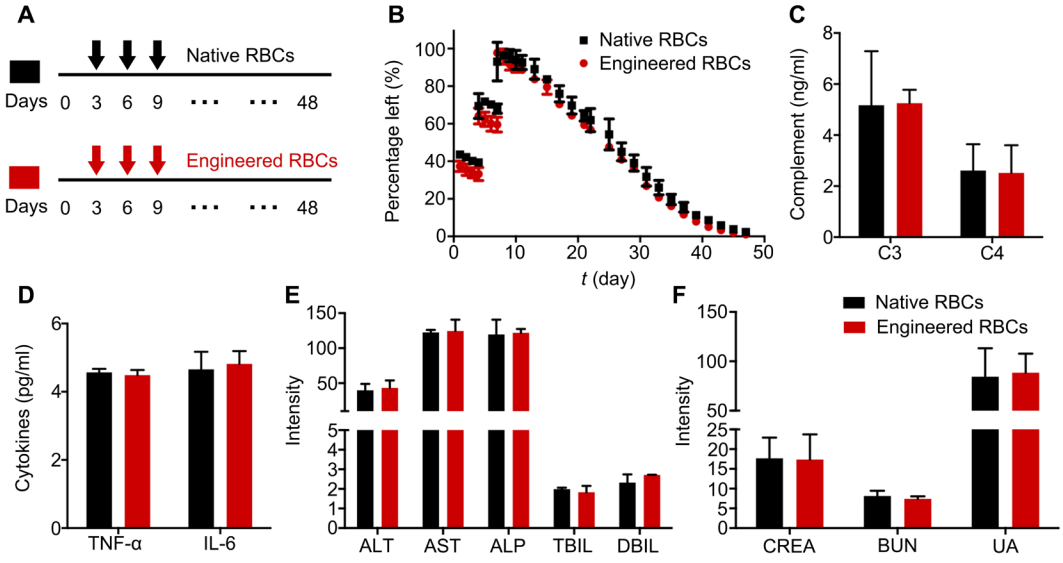

Fig. 5. Complement and cytokine assay and biochemical analysis of organ functions following multiple transfusions. (**A**) Timeline of the three succeeding blood transfusions. (**B**) Life span of PKH-26–labeled native and engineered RBCs after blood transfusion in vivo. (**C**) Serum levels of complement 3 and complement 4 after multiple transfusions. (**D**) Serum levels of TNF-α and IL-6 after multiple transfusions. (**E**) Biochemical analysis of liver function after multiple transfusions. ALT (U/l), AST (U/l), ALP (U/l), TBIL (μM), DBIL (μM). (**F**) Biochemical analysis of kidney function after multiple transfusions. CREA (μM), BUN (mM), UA (μM).

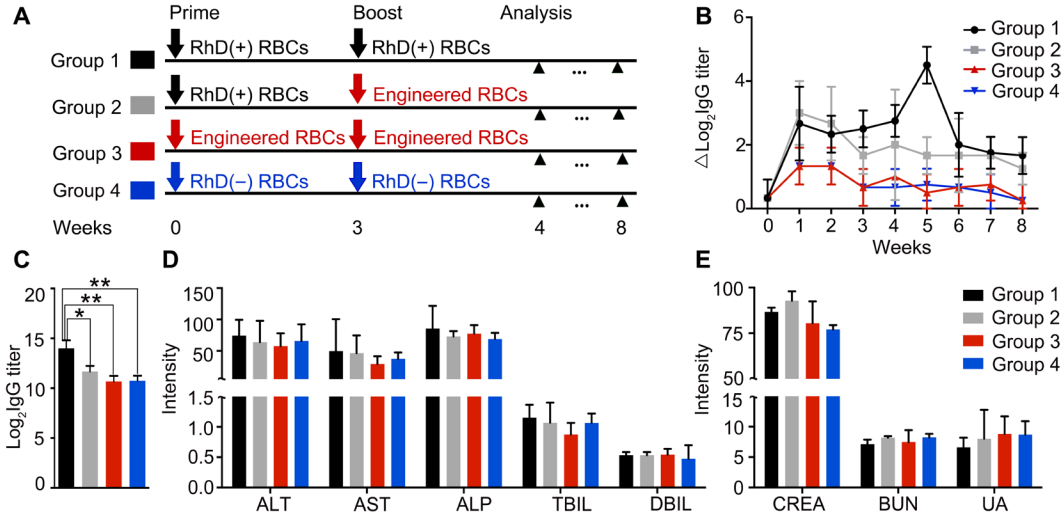

Fig. 6. Immune responses and biochemical analysis of organ functions following immunostimulation in a rabbit model. (**A**) Timeline of prime, boost, and analysis steps of the immunostimulation. (**B**) Antibody titers in rabbits after receiving immunostimulation with native human RhD-positive RBCs, engineered human RhD-positive RBCs, and human RhD-negative RBCs at different time points. (**C**) Antibody titers in rabbits during the 5th week of immunostimulation after injection in the four groups. (**D**) Biochemical analysis of liver function during the 5th week of immunostimulation after injection in the four groups. ALT (U/l), AST (U/l), ALP (U/l), TBIL (μM), DBILALT (μM). (**E**) Biochemical analysis of kidney function during the 5th week in the four groups after immunostimulation. CREA (μM), BUN (mM), UA (μM).

RBCs and their membranes have evolutionarily conserved purposes, such as localizing and protecting intracellular Hb (*34*). Thus, obscuring antigenic epitopes while leaving the RBCs structurally and functionally normal and antigenically stealthy might be more advisable. The "erase" approach may work well for the transformation of ABO blood types; however, this approach is not possible for RhD-related epitopes, which compose the original cell membrane (*9*). "Molecular brush" camouflage on the RBCs involving PEG derivatives (*11*–*14*) or PDA modifications (*16*) can attenuate antigenic recognition, although the resulting effect is incomplete.

The fluidity of the cell membrane meets the circulating demand of RBCs around the body. The surface-anchored crosslinking framework for RhD-epitope stealth RBCs can make the RhD-epitope coverage completely and antigenically stealthy, which is different from previous attempts, including PEG derivatives and PDA approach (*16*). Compared with the cell surface–anchored 3D framework reported in this study, PEG derivatives and PDA modifications all involve chemical conjugation and 2D shielding. RhD is a membrane skeleton protein anchored inside the lipid bilayer. A 3D framework anchored on the cell surface could selectively cover the membrane skeleton protein

at different altitudes in the direction perpendicular to the cell surface by modulating the layer thickness, which represents the key to RhD shielding. Complete shielding is achieved by floating the cover of the hydrogel layer on the cell surface without solidifying the cell membrane and cannot be achieved by 2D methods, such as the molecular brush technique. The 3D framework can balance the cell membrane fluidity and RhD antigen shielding, and it achieves the complete avoidance of immune responses under in vivo conditions for the first time.

In addition to the ability of the flexible texture of the 3D framework to maintain cell membrane fluidity, PSA crosslinking with biogenic amines (tyramine), which forms the framework structure, was used to construct the cellular exterior due to the potentially significant role of sialic acid in the circulation time of erythrocytes (*35*). Sialic acid can "hide" engineered RBCs with no antibody induction and keep them in the bloodstream with a long circulation time (*36*). Sialic acids occur at the ends of sugar chains connected to the surfaces of cells and cover mannose antigens on the surface of host cells or bacteria from mannose-binding lectin, which prevents complement activation (*37*, *38*). However, PEG is immunogenic in animals and humans, which is a vital problem for the usage of PEG derivatives (*35*, *39*) and PEG-lipids (*40*–*42*).

Engineering truly universal "blood group O RhD-negative" RBCs represents a "holy grail" in the blood transfusion field (*35*). The surface-anchored crosslinking framework is also effective for blood groups A and B, which provide the possibility of achieving blood group O RhD-negative RBCs. Otherwise, combined with the erase approach of enzyme for the transformation of ABO blood types, this approach can also successfully engineer the universal blood group O RhD-negative RBCs. This study provides new hope for the generation of universal blood cells based on cell surface framework engineering. More endeavors to upscale the cell engineering method to produce clinically relevant doses of RBCs for human transfusion and additional investigations of the long-term biosafety and immunogenicity of the engineered RBCs are critical before the clinical use of these RBCs in blood transfusions.

CONCLUSIONS

In summary, this study represents a complete attempt to produce RhD-epitope stealth RBCs. The resulting universal RBCs presented were generated by a simple preparation method that involves cell surface engineering and effective RBC antigen masking, and they can potentially be used for blood transfusions in emergencies. This study demonstrates a biocompatible membrane-anchoring self-assembly method for cell surface engineering. This approach may promote immunological applications by sheltering antigens of tissues and cells at the single-cell level. We believe that the application of cell surface engineering will provide an alternative strategy to preventing rejection reactions with control over cellular functions through material transformation. More generally, the concept of individual cell-material functional hybrids is explained by using the rational design presented here, providing translational insights into transfusion and transplantation medicine.

MATERIALS AND METHODS

Study design

The objective of this study was to develop a type of universal blood cell based on a cell surface–anchored 3D framework for blood transfusion in emergency situations without the need for blood type matching. Cell surface engineering of RBCs was conducted by the self-assembly of lipid-like anchor molecules, and a uniform nanogel layer composed of PSA and tyramine was generated on individual RBCs through catalysis by surface-anchored enzymes. We first characterized the results of the cellular shell on the RBCs by fluorescence identification and electron microscopy and then demonstrated that the surface-anchored framework could prevent antibody-mediated aggregation in vitro using microplate-based assays, with further identification by flow cytometry. Next, we tested the physiochemical and biofunctional properties of the engineered RBCs to confirm that the cell surface framework did not affect the key functions of the RBCs. Last, we performed blood transfusion in a mouse model and immunostimulation with human RhD-positive RBCs in a rabbit model to confirm the biocompatibility, biofunctionality, and universal stealth characteristics of the engineered RhD-negative RBCs.

Preparation of the anchor molecules and framework

To produce the anchor molecule oleyl-*O*-poly(ethylene glycol)-succinyl-*N*-hydroxyl-succinimidyl ester, designated BAMs were synthesized with 40-U repeats of ethylene oxide in the PEG moiety (Aladdin, China). BAM-HRP was prepared based on a previously reported method by mixing phosphate-buffered saline (PBS) containing 0.3% (w/v) HRP (Sigma-Aldrich) and dimethyl sulfoxide containing 0.2% (w/v) NHS-conjugated BAM (BAM-NHS). After 2 hours of mixing at room temperature, BAM-HRP was purified by filtration to remove the remaining BAM-NHS, and it was then stored at 4°C in PBS. PSA at a size of 50 kDa (molecular weight) was synthesized by fermentation using engineered *Escherichia coli* and subsequently purified by chromatography. To produce the PSA-tyramine framework, PSA was activated with *N*-(3-dimethylaminopropyl)-*N*′-ethylcarbodiimide hydrochloride (Sigma-Aldrich) and NHS (Sigma-Aldrich). The ^{1}H NMR spectra were tested on a 600 MHz Direct Drive 2 NMR spectrometer (Agilent, USA).

Cell surface engineering

Blood specimens were drawn from healthy donors after obtaining informed consent at the Second Affiliated Hospital of Zhejiang University School of Medicine under an institutional review board–approved protocol. The RBCs were separated from whole blood by centrifugation (600*g*, 5 min). RBCs (1×10^6 cells ml^{-1}) were suspended in PBS (1× PBS, 10 mM, pH 7.2) or 0.9% (w/v) NaCl, and HRP on the cell surface was immobilized by adding a BAM-HRP solution (12 μg ml^{-1}). After 10 min, the RBCs were harvested by centrifugation, washed twice with 10 mM PBS buffer, and resuspended in PBS buffer. The cells were added to a PSA-tyramine (0.5 mM) suspension in an H_2O_2 solution (10 mM) for 20 min.

Cell surface characterization

The native and engineered RBCs were fixed with 4% glutaraldehyde and washed with distilled water, and then SEM images were obtained under an S-4800 microscope (Hitachi, Japan) at an acceleration voltage of 5 kV. Biological TEM was conducted with a JEM-1230 microscope (JEOL, Japan). The samples were fixed with glutaraldehyde, OsO_4, and $K_2Cr_2O_7$, and after dehydration in ethanol/acetone, they were embedded in Epon 812/Araldite M resin. Thin sections were cut using a Reichert ultratome (Zeiss, Germany) and then stained with uranyl acetate and lead citrate. RhD-positive RBCs were encapsulated via the surface engineering method described above, and only the

alternative frameworks were covalently coupled with fluoresceinamine isomer I (Sigma-Aldrich). Then, the native and engineered RBCs were rinsed with PBS three times, cultured in PBS buffer for 1, 5, 10, 15, 20, and 25 days, and then subjected to CLSM (Nikon, Japan). All images were captured and analyzed using image analysis software (Zen Light Edition 2009). FTIR spectra were collected on a Nicolet iS10 spectrometer (Thermo Fisher Scientific) using a GS10800-B Quest sampling accessory (Specac, England) with a diamond attenuated total reflectance sampling plate to study the composition of the PSA and PSA-tyramine.

Agglutination assay

The native and engineered RBCs were plated in 96-well plates at 1×10^5 cells per well in 100 μl of 10 mM PBS. Then, 10 μl of anti-D, anti-A, and/or anti-B blood grouping reagent (monoclonal antibodies, SHPBC, China) was added to each well, and the cells were incubated for 1 hour at room temperature. Incubated cells were stirred using pipette tips and then observed using optical microscopy, and the images were captured on an Axio Observer A1 microscope (Zeiss, Germany).

Flow cytometry analysis

The native and engineered RBCs were fixed with 4% glutaraldehyde at 4°C overnight and washed twice with a 10 mM PBS buffer solution. The specimens were incubated with commercial anti-D (Rh) monoclonal antibodies (IgG; dilution, 1:10; 4A Biotech, China) or anti-B monoclonal antibodies (IgM; dilution, 1:10; ab24224, Abcam) for 1 hour at room temperature. Subsequently, the samples were washed three times with PBS and incubated with Alexa Fluor 568 goat anti-mouse IgG fluorescent dye (dilution, 1:200; ab175473, Abcam) for 2 hours at room temperature. The stained cells were analyzed using an FC500 MPL flow cytometer (Beckman Coulter, CA) and FXP software (CXP 2.1).

Analysis of physical properties

To test the osmotic fragility of the universal RBCs in vitro, the native and modified RBCs were added to saline solutions prepared with the following weight percentages of an NaCl solution: 0.900, 0.650, 0.550, 0.500, 0.475, 0.425, 0.400, 0.375, 0.350, 0.300, 0.275, 0.250, 0.150, and 0.000 (weight %). The blood samples were incubated at 37°C for 1 hour, and osmotic fragility was evaluated by measuring the absorbance of the samples at 540 nm using Drabkin's reagent (Sigma). The hemolysis assays of native and engineered RBCs were also performed using the Drabkin's reagent (Sigma) by testing the absorbance of the supernatant at 540 nm. The deformability of the native RBC and engineered RBC samples was measured using an LBY-BX2 ektacytometer (Precil, China) at a shear rate of 50 to 1000 s^{-1}. The native and engineered samples were each diluted in 5 ml of a 4% polyvinylpyrrolidone solution (molecular weight, 360 kDa) to obtain 2×10^7 cells ml^{-1} for ektacytometry. Photometric measurements generated a signal termed the deformability index (DI), and the value of the DI at the maximum shear rate of 1000 s^{-1} was designated the DI_{max}. The zeta potentials of the native and engineered RBCs were determined using Zetasizer Nano S (Malvern, UK). The cell densities of the native and engineered RBCs were approximately 1×10^6 cells ml^{-1} in 10 mM PBS buffer (pH 7.2) when they were tested. The hydrophobicity of the membranes of the native and engineered RBCs was measured by monitoring the evolution of the contact angle with an OCA15+ instrument (DataPhysics, Germany). The native and engineered cells were sampled on a clean and hydrophilic silicon wafer with a sessile drop of distilled water on the substrates.

Biological function analysis of the RBCs

The oxygen affinity and Hill plots of the native and engineered RBCs were calculated from an oxygen equilibrium curve measured with a Hemox analyzer (TCS Scientific, CA) at 37°C. The samples were diluted with PBS (pH 7.2, 37°C). The 2,3-DPG content in the RBCs before and after the framework modifications was quantified using a 2,3-DPG test kit (Sigma). The ATP content was also investigated after framework engineering using the ENLITEN ATP Assay System (Promega, CA). The UV-Vis absorption spectra were measured using a T6 UV-Vis spectrometer (Puxi, China). The Lorrca system (Mechatronics) was used to determine all the aggregation measurements of native RBCs, engineered RBCs, and mixtures of native and engineered RBCs by syllectometry. Human umbilical vein endothelial cells (HUVECs) were cultured in Dulbecco's modified Eagle's medium supplemented with 10% fetal bovine serum, maintained at 37°C in humidified air and 5% CO_2, and used for the flow adhesion experiments. The HUVECs were cultured in a flow chamber (ibidi, Germany), examined using an Eclipse TE2000-S microscope (Nikon, Japan), and perfused with native RBCs, engineered RBCs, and mixtures of native and engineered RBCs at a shear rate of 1.5 dynes/cm for 20 min and then with cell-free solution for rinsing at the same shear rate. The assays of clot dynamics parameters (R, K, α, and MA) were performed using the TEG test (TCA 6000, China).

In vivo distribution in blood transfusion

All handling and care of animals were performed according to the guidelines on the care and use of animals for scientific purposes issued by Zhejiang University. The distribution of native and engineered mouse RBCs was examined in vivo in mice obtained from Institute of Cancer Research (ICR). Whole blood was acquired from different donor mice and washed with 10 mM PBS, with erythrocytes collected by centrifugation. Half of the RBCs were engineered with frameworks as described above, and the same volume of native RBCs was labeled with DIR dye (GeneCopoeia, MD). Labeled RBCs (200 μl, 1×10^9 cells ml^{-1}) were intravenously injected into each recipient mouse ($n = 3$, in each group). The DIR dye signals were subjected to Vevo LAZR imaging (Visual Sonics, Canada) to measure the RBCs' distribution in the major organs (heart, liver, spleen, and kidneys). The in vivo survival assay of the RBCs was carried out during the same process, although the dye was substituted with PKH-26 (Sigma), which is a fluorescence molecule that can label the cell membrane. The survival profiles of RBCs were tested and recorded until no signals were determined by detecting the PKH-26 fluorescence using a FC500 MPL flow cytometer (Beckman Coulter, CA). Approximately 0.5 ml of whole blood from each mouse was harvested for routine blood tests by eyeball extirpation. The major organs (heart, liver, spleen, lung, and kidneys) were harvested and fixed in a 10% formalin solution. For histopathological examinations, the tissue samples were embedded in paraffin blocks, sectioned into slices, and mounted onto glass slides. After H&E staining, images were captured via Eclipse TE2000-S microscopy (Nikon, Japan). The serum levels of complement 3 (MU30594, Bioswamp), complement 4 (MU30595, Bioswamp), TNF-α (ab208348, Abcam), and IL-6 (ab100712, Abcam) were determined using an ELISA kit.

The ICR mice removed 200 μl of blood from the retro-orbital sinus, and then an equal volume of native (type-matched) or engineered RBCs was intravenously injected. HR, MBP, and SBP were tested using a BP-98A mice noninvasive sphygmomanometer (Softron, Japan).

In vivo immunogenicity evaluation in immunostimulation

The evaluations of immunogenicity were performed in vivo using New Zealand white rabbits. The rabbits were randomly divided into four groups (n = 5) for the evaluation of immunogenicity. The treatment of the rabbits in group 1 consisted of an intraperitoneal injection of 500 μl of RhD-positive RBCs and a second intraperitoneal injection of 500 μl of RhD-positive RBCs after 3 weeks. The treatment of the rabbits in group 2 consisted of an intraperitoneal injection of 500 μl of RhD-positive RBCs and a second intraperitoneal injection of 500 μl of engineered RBCs after 3 weeks. The treatment of the rabbits in group 3 consisted of an intraperitoneal injection of 500 μl of engineered RBCs and a second intraperitoneal injection of 500 μl of engineered RBCs after 3 weeks. The treatment of the rabbits in group 4 consisted of an intraperitoneal injection of 500 μl of RhD-negative RBCs and a second intraperitoneal injection of 500 μl of RhD-negative RBCs after 3 weeks. Sera samples were collected every week. ELISAs were performed to analyze both framework and nonframework binding to RhD-positive RBCs and assess the RhD antibody titers in vivo. Briefly, recombinant human RhD proteins (ab80087, Abcam) were used to coat ELISA plates (Corning, NY) at 2 μg ml^{-1} in 100 μl of coating solution at pH 9.6 (0.05 M bicarbonate buffer). After overnight incubation at 4°C, the plates were washed three times with PBS containing 0.2% (v/v) Tween (Tween 20, Sigma) [PBS + 0.2% Tween (PBST)] and blocked with blocking buffer (Beyotime, China) for 2 hours at 37°C. The plates were then washed three times, and 100 μl of the sera samples was added. After 1 hour of incubation at 37°C, the plates were washed three times and 100 μl of HRP-conjugated secondary antibody (ab6721, Abcam; dilution, 1:100,000) was added. After 45 min of incubation at 37°C, the plates were washed three times, and 100 μl of TMB chromogen substrate solution (Beyotime, China) was added. Regarding the end-point titers, 50 μl of 1 M H_2SO_4 was added after 10 min to stop the reaction. The absorbance was measured at 450 nm using a microplate reader (BioTek, USA).

Statistical analysis

All data were analyzed using Student's t test and are presented as means ± SD of at least quadruplicate samples from independent analyses, as indicated. *$P < 0.05$ was considered to indicate a significant difference, and **$P < 0.01$ was considered to be highly significant. Statistical tests were performed with GraphPad Prism software (La Jolla, CA).

SUPPLEMENTARY MATERIALS

Supplementary material for this article is available at http://advances.sciencemag.org/cgi/content/full/6/12/eaaw9679/DC1

Supplementary Materials and Methods

Fig. S1. Chemical characterizations of the enzymatically crosslinked framework for the encapsulation of the universal RBCs.

Fig. S2. Stability of the engineered universal RBCs in human plasma.

Fig. S3. Effects of the PSA-tyramine concentration on the optimized engineering of universal RBCs to prevent antibody-mediated aggregation in multiple blood types.

Fig. S4. Anti-RhD antibody–mediated human RhD-positive RBC aggregation via different methods of cell surface engineering.

Fig. S5. Cytomechanical and biochemical analysis, Bohr coefficient of the Hb forms in different circumstances, and blood clotting function of the native and engineered RBCs.

Fig. S6. Organ distribution and in vivo functional profiles of the native and engineered RBCs illustrated by the imaging function of the photoacoustic system.

Fig. S7. Biological safety evaluation of blood transfusion with native and engineered RBCs in a mouse model.

Fig. S8. Rescue experiment for the hemorrhagic test via the transfusion of native and engineered RBCs in a mouse model.

Table S1. Routine blood assays of the mice transfused with the native and engineered RBCs.

Table S2. Routine blood assays for the hemorrhagic test after the transfusion with the native and engineered RBCs.

View/request a protocol for this paper from *Bio-protocol*.

REFERENCES AND NOTES

1. K. Landsteiner, Agglutination phenomena in normal human-blood (reprinted from wiener-klinische-wochenschrift, vol 14, p 1132, 1901). *Wien. Klin. Wochenschr.* **100**, 257–258 (1988).
2. G. Daniels, in *Human Blood Groups* (Wiley-Blackwell, 2013), pp. 1–10.
3. S. T. Chou, T. Jackson, S. Vege, K. Smith-Whitley, D. F. Friedman, C. M. Westhoff, High prevalence of red blood cell alloimmunization in sickle cell disease despite transfusion from rh-matched minority donors. *Blood* **122**, 1062–1071 (2013).
4. N. D. Avent, M. E. Reid, The rh blood group system: A review. *Blood* **95**, 375–387 (2000).
5. S. Simsek, B. H. Faas, P. M. Bleeker, M. A. Overbeeke, H. T. Cuijpers, C. E. van der Schoot, A. E. von dem Borne, Rapid Rh-D genotyping by polymerase chain reaction-based amplification of DNA. *Blood* **85**, 2975–2980 (1995).
6. S. G. Ahmed, A strategic approach to the problems of providing rhesus d-negative blood transfusion in geographic areas with low rhd negativity: A nigerian perspective. *Transfus. Med. Rev.* **24**, 140–146 (2010).
7. J. Goldstein, G. Siviglia, R. Hurst, L. Lenny, L. Reich, Group-b erythrocytes enzymatically converted to group-o survive normally in A, B, and O individuals. *Science* **215**, 168–170 (1982).
8. Q. P. Liu, G. Sulzenbacher, H. Yuan, E. P. Bennett, G. Pietz, K. Saunders, J. Spence, E. Nudelman, S. B. Levery, T. White, J. M. Neveu, W. S. Lane, Y. Bourne, M. L. Olsson, B. Henrissat, H. Clausen, Bacterial glycosidases for the production of universal red blood cells. *Nat. Biotechnol.* **25**, 454–464 (2007).
9. M. Salomao, X. Zhang, Y. Yang, S. Lee, J. H. Hartwig, J. A. Chasis, N. Mohandas, X. An, Protein 4.1r-dependent multiprotein complex: New insights into the structural organization of the red blood cell membrane. *Proc. Natl. Acad. Sci. U.S.A.* **105**, 8026–8031 (2008).
10. Y.-H. Kim, H. O. Kim, E. J. Baek, R. Kurita, H.-J. Cha, Y. Nakamura, H. Kim, Rh d blood group conversion using transcription activator-like effector nucleases. *Nat. Commun.* **6**, 8678 (2015).
11. M. D. Scott, K. L. Murad, F. Koumpouras, M. Talbot, J. W. Eaton, Chemical camouflage of antigenic determinants: Stealth erythrocytes. *Proc. Natl. Acad. Sci. U.S.A.* **94**, 7566–7571 (1997).
12. N. A. A. Rossi, I. Constantinescu, D. E. Brooks, M. D. Scott, J. N. Kizhakkedathu, Enhanced cell surface polymer grafting in concentrated and nonreactive aqueous polymer solutions. *J. Am. Chem. Soc.* **132**, 3423–3430 (2010).
13. N. A. A. Rossi, I. Constantinescu, R. K. Kainthan, D. E. Brooks, M. D. Scott, J. N. Kizhakkedathu, Red blood cell membrane grafting of multi-functional hyperbranched polyglycerols. *Biomaterials* **31**, 4167–4178 (2010).
14. D. Wang, W. M. Toyofuku, M. D. Scott, The potential utility of methoxypoly(ethylene glycol)-mediated prevention of rhesus blood group antigen rhd recognition in transfusion medicine. *Biomaterials* **33**, 3002–3012 (2012).
15. S. Mansouri, Y. Merhi, F. M. Winnik, M. Tabrizian, Investigation of layer-by-layer assembly of polyelectrolytes on fully functional human red blood cells in suspension for attenuated immune response. *Biomacromolecules* **12**, 585–592 (2011).
16. B. Wang, G. Wang, B. Zhao, J. Chen, X. Zhang, R. Tang, Antigenically shielded universal red blood cells by polydopamine-based cell surface engineering. *Chem. Sci.* **5**, 3463–3468 (2014).
17. S. Sakai, M. Taya, On-cell surface cross-linking of polymer molecules by horseradish peroxidase anchored to cell membrane for individual cell encapsulation in hydrogel sheath. *ACS Macro Lett.* **3**, 972–975 (2015).
18. K. Kato, C. Itoh, T. Yasukouchi, T. Nagamune, Rapid protein anchoring into the membranes of mammalian cells using oleyl chain and poly(ethylene glycol) derivatives. *Biotechnol. Prog.* **20**, 897–904 (2004).
19. R. Jin, C. Hiemstra, Z. Zhong, J. Feijen, Enzyme-mediated fast in situ formation of hydrogels from dextran-tyramine conjugates. *Biomaterials* **28**, 2791–2800 (2007).
20. N. Li, A. Than, X. Wang, S. Xu, L. Sun, H. Duan, C. Xu, P. Chen, Ultrasensitive profiling of metabolites using tyramine-functionalized graphene quantum dots. *ACS Nano* **10**, 3622–3629 (2016).
21. E. Beutler, W. Kuhl, C. West, The osmotic fragility of erythrocytes after prolonged liquid storage and after reinfusion. *Blood* **59**, 1141–1147 (1982).
22. M. Morse, D. E. Cassels, M. Holder, E. O'Connell, A. Swanson, The position of the oxygen dissociation curve of the blood in normal children and adults. *J. Clin. Invest.* **29**, 1091–1097 (1950).
23. E. Rumi, F. Passamonti, L. Pagano, M. Ammirabile, L. Arcaini, C. Elena, A. Flagiello, R. Tedesco, C. Vercellati, A. P. Marcello, D. Pietra, R. Moratti, M. Cazzola, M. Lazzarino, Blood p50 evaluation enhances diagnostic definition of isolated erythrocytosis. *J. Intern. Med.* **265**, 266–274 (2009).

24. B. R. Wood, S. J. Langford, B. M. Cooke, J. Lim, F. K. Glenister, M. Duriska, J. K. Unthank, D. McNaughton, Resonance raman spectroscopy reveals new insight into the electronic structure of beta-hematin and malaria pigment. *J. Am. Chem. Soc.* **126**, 9233–9239 (2004).
25. T. Yonetani, S. Park, A. Tsuneshige, K. Imai, K. Kanaori, Global allostery model of hemoglobin - modulation of o-2 affinity, cooperativity, and bohr effect by heterotropic allosteric effectors. *J. Biol. Chem.* **277**, 34508–34520 (2002).
26. H. F. Bunn, R. W. Briehl, The interaction of 2,3-diphosphoglycerate with various human hemoglobins. *J. Clin. Invest.* **49**, 1088–1095 (1970).
27. Y. Park, C. A. Best, T. Auth, N. S. Gov, S. A. Safran, G. Popescu, S. Suresh, M. S. Feld, Metabolic remodeling of the human red blood cell membrane. *Proc. Natl. Acad. Sci. U.S.A.* **107**, 1289–1294 (2010).
28. Y. Izumida, A. Seiyama, N. Maeda, Erythrocyte aggregation: Bridging by macromolecules and electrostatic repulsion by sialic acid. *Biochim. Biophys. Acta* **1067**, 221–226 (1991).
29. R. P. Hebbel, M. A. B. Boogaerts, J. W. Eaton, M. H. Steinberg, Erythrocyte adherence to endothelium in sickle-cell anemia. A possible determinant of disease severity. *N. Engl. J. Med.* **302**, 992–995 (1980).
30. G. Eduardo, F. M. Pieracci, E. E. Moore, J. L. Kashuk, Coagulation abnormalities in the trauma patient: The role of point-of-care thromboelastography. *Semin. Thromb. Hemost.* **36**, 723–737 (2010).
31. E. P. Vichinsky, A. Earles, R. A. Johnson, M. S. Hoag, A. Williams, B. Lubin, Alloimmunization in sickle-cell-anemia and transfusion of racially unmatched blood. *N. Engl. J. Med.* **322**, 1617–1621 (1990).
32. C. P. Shao, Transfusion of RhD-positive blood in "Asia type" DEL recipients. *N. Engl. J. Med.* **362**, 472–473 (2010).
33. C. Natanson, S. J. Kern, P. Lurie, S. M. Banks, S. M. Wolfe, Cell-free hemoglobin-based blood substitutes and risk of myocardial infarction and death - a meta-analysis. *JAMA* **299**, 2304–2312 (2008).
34. A. I. Alayash, Blood substitutes: Why haven't we been more successful? *Trends Biotechnol.* **32**, 177–185 (2014).
35. G. Garratty, Modulating the red cell membrane to produce universal/stealth donor red cells suitable for transfusion. *Vox Sang* **94**, 87–95 (2008).
36. D. Aminoff, W. F. Bruegge, W. C. Bell, K. Sarpolis, R. Williams, Role of sialic acid in survival of erythrocytes in the circulation: Interaction of neuraminidase-treated and untreated erythrocytes with spleen and liver at the cellular level. *Proc. Natl. Acad. Sci. U.S.A.* **74**, 1521–1524 (1977).
37. M. M. Fuster, J. D. Esko, The sweet and sour of cancer: Glycans as novel therapeutic targets. *Nat. Rev. Cancer* **5**, 526–542 (2005).
38. E. Severi, D. W. Hood, G. H. Thomas, Sialic acid utilization by bacterial pathogens. *Microbiology* **153**, 2817–2822 (2007).
39. C.-J. Chang, C.-H. Chen, B.-M. Chen, Y.-C. Su, Y.-T. Chen, M. S. Hershfield, M.-T. M. Lee, T.-L. Cheng, Y.-T. Chen, S. R. Roffler, J.-Y. Wu, A genome-wide association study identifies a novel susceptibility locus for the immunogenicity of polyethylene glycol. *Nat. Commun.* **8**, 522 (2017).
40. S. Miura, Y. Teramura, H. Iwata, Encapsulation of islets with ultra-thin polyion complex membrane through poly(ethylene glycol)-phospholipids anchored to cell membrane. *Biomaterials* **27**, 5828–5835 (2006).
41. Y. Teramura, Y. Kaneda, H. Iwata, Islet-encapsulation in ultra-thin layer-by-layer membranes of poly(vinyl alcohol) anchored to poly(ethylene glycol)-lipids in the cell membrane. *Biomaterials* **28**, 4818–4825 (2007).
42. Y. Teramura, O. P. Oommen, J. Olerud, J. Hilborn, B. Nilsson, Microencapsulation of cells, including islets, within stable ultra-thin membranes of maleimide-conjugated peg-lipid with multifunctional crosslinkers. *Biomaterials* **34**, 2683–2693 (2013).

Acknowledgments: We thank X. Wang from Chongqing University for providing the analysis platform of RBCs and Y. Chen, D. Xu, and M. Xie from the Laboratory Animal Centre for assistance with the animal experiments. We are grateful to the staff of the Core Facilities in the Institute of Translational Medicine of Zhejiang University for assisting with flow cytometry, CLSM, microplate spectrophotometry, and fluorescence microscopy. **Funding:** This study was supported by grants from the National Natural Science Foundation of China (81570168, 21625105, and 31822019), the National Key R&D Program of China (2016YFC1100800 and 2016YFA0203600), and the Distinguished Young Scientist Award from the Natural Science Foundation of Zhejiang Province (LR16H180001). **Author contributions:** R.T. and B.W. conceived and directed the study. Y.Z. contributed to all experimental work and the data analyses. Y.Z., M.F., and Y.C. carried out the animal experiments. Z. Liu performed the FTIR and zeta potential analysis. C.S. performed the SEM and contact angle measurements. B.J. performed the TEM measurements. L.H. helped with the ODC measurements. S.W. and D.L. helped with in vivo imaging of the photoacoustic system. Z. Liao helped with the TEG measurements. Y.Z., R.T., and B.W. wrote the manuscript. All authors discussed and commented on the manuscript. **Competing interests:** B.W., Y.Z., M.F., and R.T. are inventors on the patent application (201710908231.6) filed on the basis on this work. The remaining authors declare that they have no competing interests. **Data and materials availability:** All data needed to evaluate the conclusions in the paper are present in the paper and/or the Supplementary Materials. Additional data related to this paper may be requested from the authors.

Submitted 11 February 2019
Accepted 26 December 2019
Published 20 March 2020
10.1126/sciadv.aaw9679

Citation: Y. Zhao, M. Fan, Y. Chen, Z. Liu, C. Shao, B. Jin, X. Wang, L. Hui, S. Wang, Z. Liao, D. Ling, R. Tang, B. Wang, Surface-anchored framework for generating RhD-epitope stealth red blood cells. *Sci. Adv.* **6**, eaaw9679 (2020).